

# Long-Term Stability of Ammonia Decomposition over Nickel-Based Catalysts

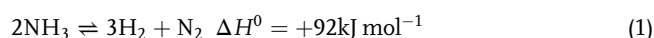
Maximilian Purcel, Astrid Sophie Müller, Patrick Diehl, Konstantinos Kappis, Annette Trunschke, and Martin Muhler\*

Green hydrogen can be used as the backbone of a novel energy system and as a feedstock for renewable chemistry. H<sub>2</sub> storage and transport are challenging, but ammonia as a hydrogen carrier could potentially solve these inefficiencies. Many studies focus on high catalytic activities, but the long-term stability is often insufficiently investigated. This work reports on the stability of a nickel-based reference catalyst and a coprecipitated Ni/Al<sub>2</sub>O<sub>3</sub> catalyst over 800 h time on stream (TOS) in 98% NH<sub>3</sub> at atmospheric pressure. An automated temperature control is necessary to adjust the temperature of the heat source to compensate for the changing heat demand resulting from catalyst activation or deactivation. Under reaction conditions the reference catalyst first undergo an activation phase before reaching its maximum conversion of 91.9% after 250 h TOS followed by a minor decrease in conversion. In comparison, the Ni/Al<sub>2</sub>O<sub>3</sub> catalyst shows lower activity and undergo a continuous deactivation due to sintering. Overall, the activity loss at 534 °C amounted to only 1.5% for the reference catalyst and to 13.5% for the Ni/Al<sub>2</sub>O<sub>3</sub> catalyst compared with the maximum conversion level. Thus, the Ni-based reference catalyst proves to be very stable under industrially relevant NH<sub>3</sub> decomposition conditions.

reforming of fossil fuels, especially natural gas.<sup>[2,3]</sup> Steam reforming produces 10 621 gCO<sub>2</sub>/kgH<sub>2</sub> which accounts for roughly 90% of the global warming potential of this process in addition to mostly methane emission.<sup>[4]</sup> An alternative would be the production of green hydrogen using renewable energies and feedstocks.<sup>[5]</sup> However, storage and transport of H<sub>2</sub> is a challenging task since H<sub>2</sub> has a high mass-related energy density, but a very low volumetric energy density.<sup>[6,7]</sup>

The storage of H<sub>2</sub> by converting it to NH<sub>3</sub> is a promising technology, since NH<sub>3</sub> contains 17.8% of hydrogen by weight (121 kg H<sub>2</sub> m<sup>-3</sup> at 10 bar)<sup>[8]</sup> and can be easily liquified (8.6 bar at 20 °C).<sup>[9]</sup> Due to the narrow combustion range of NH<sub>3</sub> (16–25% in air) compared with H<sub>2</sub>, the storage of H<sub>2</sub> using NH<sub>3</sub> can also be beneficial with regard to safety.<sup>[10,11]</sup> The potential of NH<sub>3</sub> as a hydrogen carrier and potential applications were recently reviewed by Ristig et al.<sup>[12]</sup>

When using NH<sub>3</sub> as H<sub>2</sub> carrier, the catalytic decomposition of NH<sub>3</sub> back to H<sub>2</sub> as a key step has to be improved.<sup>[13]</sup>



The non-oxidative decomposition of NH<sub>3</sub> is an endothermic process corresponding to the reverse Haber–Bosch process that is used for NH<sub>3</sub> synthesis over Fe- and Ru-based catalysts.<sup>[14]</sup> Fe- and Ru-based catalysts are promising NH<sub>3</sub> decomposition catalysts, since they are highly active in NH<sub>3</sub> synthesis, although they do not necessarily have the best catalytic properties for the decomposition according to Boisen et al.<sup>[15]</sup> Recently, Ristig et al.<sup>[12]</sup> identified Ni as promising catalyst for the decomposition of NH<sub>3</sub> due to its medium activity, low cost, and high abundance.<sup>[12]</sup>

For choosing a suitable catalyst the catalytic activity is an important criterion, but the catalyst has also to be stable over long periods of time on stream (TOS). Unfortunately, long-term stability is often a criterium that is not sufficiently investigated in most studies.

In this work we report on the experimental setup that was constructed to perform such a long-term stability test in an integral plug flow reactor (PFR) and how to investigate the stability of catalysts in NH<sub>3</sub> decomposition under steady-state conditions. A Ni-based industrial reference catalyst was selected and its


## 1. Introduction

The dependence of our current energy system on fossil fuels with its negative influence on the environment is a major challenge.<sup>[1]</sup> Nowadays, most of the H<sub>2</sub> production is still based on the steam

M. Purcel, M. Muhler  
Max Planck Institute for Chemical Energy Conversion  
45470 Mülheim an der Ruhr, Germany  
E-mail: martin.muhler@ruhr-uni-bochum.de

M. Purcel, A. S. Müller, P. Diehl, M. Muhler  
Laboratory of Industrial Chemistry  
Ruhr University Bochum  
44780 Bochum, Germany

K. Kappis, A. Trunschke  
Department of Inorganic Chemistry  
Fritz Haber Institute of the Max Planck Society  
Berlin 14195, Germany

 The ORCID identification number(s) for the author(s) of this article can be found under <https://doi.org/10.1002/ente.202400678>.

© 2024 The Authors. Energy Technology published by Wiley-VCH GmbH. This is an open access article under the terms of the Creative Commons Attribution License, which permits use, distribution and reproduction in any medium, provided the original work is properly cited.

DOI: 10.1002/ente.202400678

behavior over 796 h was investigated. To evaluate its long-term stability the changes in NH<sub>3</sub> conversion were monitored under isothermal conditions. In comparison, the long-term stability test was additionally performed with a Ni/Al<sub>2</sub>O<sub>3</sub> catalyst prepared by co-precipitation, which was characterized to identify changes under reaction conditions.

## 2. Results and Discussion

### 2.1. Long-Term NH<sub>3</sub> Decomposition Experiments

To test the temperature control system a first experiment with the reference catalyst was performed as shown in **Figure 1**. 490 mL min<sup>-1</sup> NH<sub>3</sub> and 10 mL min<sup>-1</sup> Ar were passed through 500 mg of freshly reduced catalyst, and the furnace setpoint, the catalyst temperature measured with axial thermocouple 4 and the effluent mole fraction of NH<sub>3</sub> were recorded. The setpoint for the three-point controller was set to 534 °C.

Figure 1 shows that the temperature control system adjusted the furnace setpoint successfully to keep the catalyst bed isothermal within an error margin of ±0.5 °C. The furnace setpoint was increased automatically to compensate for the increasing heat demand when conversion increased as indicated by the decrease of the NH<sub>3</sub> effluent mole fraction. Accordingly, the furnace setpoint was also lowered when conversion decreased due to deactivation, ensuring isothermal conditions during the long-term measurement.

For the calculation of the conversion of NH<sub>3</sub>, the volume expansion had to be considered. Conversion can be calculated according to Equation (2) with the initial mole fraction  $y_{\text{NH}_3,0}$  (deviating from 1 due to the internal standard Ar) and the actual NH<sub>3</sub> mole fraction  $y_{\text{NH}_3}$  in the effluent.

$$X_{\text{NH}_3} = \frac{1 - \frac{y_{\text{NH}_3}}{y_{\text{NH}_3,0}}}{1 + y_{\text{NH}_3}} \quad (2)$$

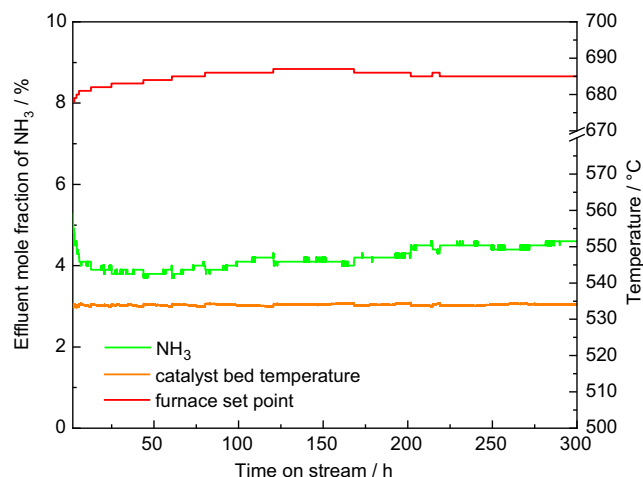


**Figure 1.** Temperature control test results using 490 mL min<sup>-1</sup> NH<sub>3</sub> and 10 mL min<sup>-1</sup> Ar, 500 mg reference catalyst, and a setpoint of 534 °C for the three-point controller.

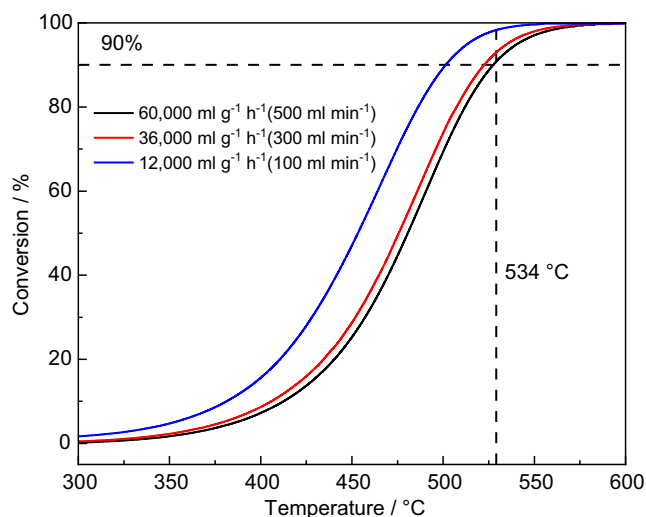


**Figure 2.** Conversion of NH<sub>3</sub> over the reference catalyst as a function of temperature at 100, 300, and 500 mL min<sup>-1</sup>. The dashed lines indicate the catalyst bed temperatures needed to obtain a conversion of 90%.

The results of the transient experiment run prior to the long-term measurement for the reference catalyst are shown in **Figure 2**.

The conversion of NH<sub>3</sub> was determined for three different flow rates as a function of temperature recorded by axial thermocouple 4. The results show that a temperature of 534 °C was needed under the conditions chosen for the long-term experiment using a feed flow rate of 500 mL min<sup>-1</sup> ( $y_{\text{NH}_3,0} = 0.98$ ).

The conversion of NH<sub>3</sub> over the Ni-based reference catalyst under isothermal conditions is shown in **Figure 3**, which was derived using the NH<sub>3</sub> mole fraction detected by gas chromatography (GC) according to Equation (2). Within the first hour on stream conversion increased from ≈80% to 91.3%. Over the course of the first 250 h on stream a slight further increase in conversion was observed to a conversion of 91.9%. After 250 h a minor deactivation of the reference catalyst was observed indicated by the decrease in conversion to 90.4% after 800 h TOS. Deactivation seems to occur linearly as suggested by the dotted line, but it cannot be excluded that it converges to a plateau beyond 800 h. Fluctuations in conversion occurred presumably due to the temperature control. Considering the uncertainties of the GC measurement the trend in catalytic activity over TOS is clear, and fluctuations are barely visible without magnification. Overall, the Ni-based reference catalyst lost only 1.5% of its activity over the course of 550 h compared with the maximum conversion of 91.9%. Relative to the conversion after 4 h TOS, only a decrease in conversion of 1.1% was observed within 796 h.

Figure 3 also shows the conversion of NH<sub>3</sub> over Ni/Al<sub>2</sub>O<sub>3</sub> prepared by co-precipitation without promoters in comparison to the reference catalyst at the same temperature. A maximum degree of NH<sub>3</sub> conversion of 54.1% at 534 °C was reached, and over the whole period of the long-term stability experiment deactivation of the Ni/Al<sub>2</sub>O<sub>3</sub> catalyst was observed. The total deactivation over 800 h TOS amounted to a loss of 13.5% relative to the maximum conversion. Due to the stronger deactivation,

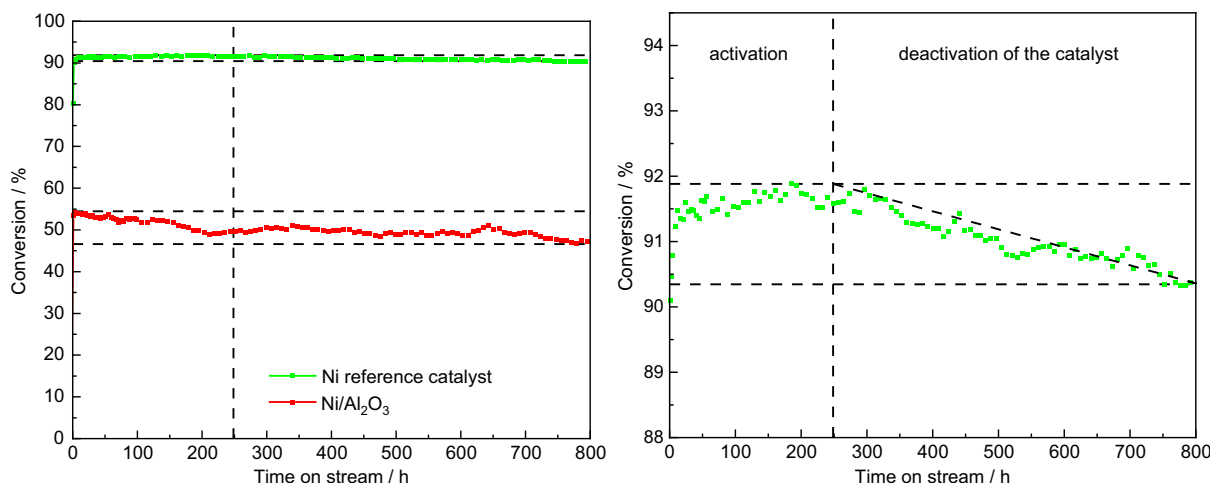


**Figure 3.** NH<sub>3</sub> conversion over 800 h TOS using the reference catalyst and the Ni/Al<sub>2</sub>O<sub>3</sub> catalyst (left). Conversion of NH<sub>3</sub> over the reference catalyst divided in an activation and deactivation period under isothermal conditions (534 °C) (right).

also the thermal effects were stronger leading to increased fluctuations in the conversion of NH<sub>3</sub>. Thus, the Ni-based reference catalyst shows much higher stability resulting in only a slight loss of activity during 800 h of steady-state operation.

## 2.2. Characterization of the Ni/Al<sub>2</sub>O<sub>3</sub> Catalyst

The temperature-programmed reduction (TPR) profile of the mixed metal oxide precursor is shown in Figure S1, Supporting Information, which consists of single reduction step from NiO to Ni<sup>0</sup> with a maximum H<sub>2</sub> consumption at 640 °C. The consumption of H<sub>2</sub> started to increase above 300 °C in good agreement with the findings of Rodriguez et al.<sup>[16]</sup> Using wavelength dispersive X-ray fluorescence (XRF), the Ni content of the calcined mixed metal precursor was determined to be 51.2 wt% close to the target value of 50 wt%.

The XRD results are shown in Figure 4 using the mixed metal oxide precursor, the reduced and passivated Ni/Al<sub>2</sub>O<sub>3</sub> sample, and the passivated catalyst after 1000 h TOS. The mixed metal oxide precursor is predominantly composed of NiO, as shown by its characteristic reflections. Upon reduction, distinct reflections indicating the presence of metallic Ni<sup>0</sup> appear confirming successful reduction. After 1000 h TOS, Ni<sup>0</sup> remains the dominant phase, but a notable shift of the reflection at 66° to higher 2θ values suggests the additional formation of Ni–Al<sub>2</sub>O<sub>4</sub> presumably during passivation. The broad reflections indicate small particle sizes and lattice disorder. Furthermore, there are no indications of nickel nitride formation under reaction conditions. The Scherrer analysis of the Ni crystallite size performed on the Ni<sup>0</sup> reflection at 52° showed average crystallite sizes of 3.5 nm for the freshly reduced and 5.0 nm for the spent catalyst after 1000 h TOS, pointing to deactivation by sintering of the Ni<sup>0</sup> nanoparticles.

N<sub>2</sub> physisorption analysis revealed a specific surface area of 275 m<sup>2</sup> g<sup>-1</sup> for the mixed metal oxide catalyst precursor. The freshly reduced and passivated Ni/Al<sub>2</sub>O<sub>3</sub> catalyst had a specific surface area of 169 m<sup>2</sup> g<sup>-1</sup>, whereas after 1000 h TOS an even

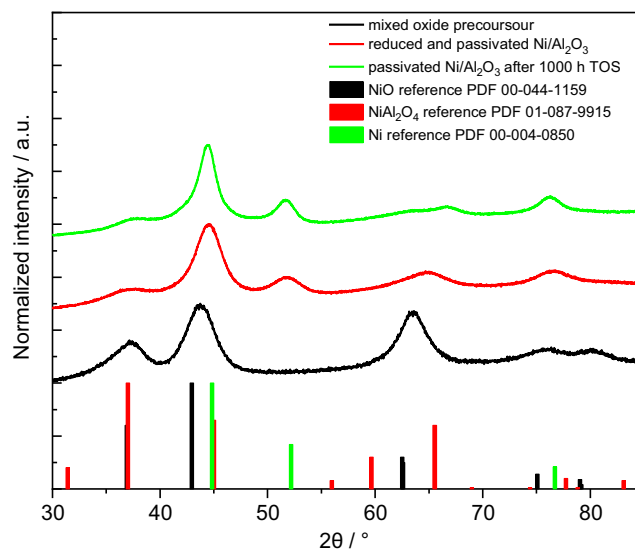


**Figure 4.** XRD patterns of the mixed NiO–Al<sub>2</sub>O<sub>3</sub> precursor, freshly reduced Ni/Al<sub>2</sub>O<sub>3</sub> and Ni/Al<sub>2</sub>O<sub>3</sub> after 1000 h TOS, both after passivation in 0.33 vol% N<sub>2</sub>O in N<sub>2</sub>.

lower specific surface area of 150 m<sup>2</sup> g<sup>-1</sup> was found. The corresponding N<sub>2</sub> physisorption isotherms are shown in Figure S2, Supporting Information. All stages of the catalyst showed type IV isotherms with a H1 hysteresis indicating the presence of uniform mesopores with a narrow size range.<sup>[17]</sup> Barrett-Joyner-Halenda (BJH) analysis of the three stages showed the different porosities of the Ni/Al<sub>2</sub>O<sub>3</sub> catalyst (Table 1).

During the reduction of NiO–Al<sub>2</sub>O<sub>3</sub> the catalyst lost 61% of its total surface area, and after 1000 h TOS the specific surface area was 11% smaller than that of the freshly reduced and passivated catalyst. Thus, the loss of catalytic activity is clearly correlated with the sintering of the alumina matrix stabilizing the Ni<sup>0</sup> nanoparticles.

**Table 1.** Results of the BET and BJH analyses of the N<sub>2</sub> physisorption isotherms of all three stages of the Ni/Al<sub>2</sub>O<sub>3</sub> catalyst.

Catalyst stage	Specific surface area	Pore volume	Pore diameter
	[m <sup>2</sup> g <sup>-1</sup> ]	[mL g <sup>-1</sup> ]	[nm]
Mixed metal oxide	275	0.604	5.4
Reduced and passivated Ni/Al <sub>2</sub> O <sub>3</sub>	169	0.296	4.7
Passivated Ni/Al <sub>2</sub> O <sub>3</sub> after 1000 h TOS	150	0.319	5.4

### 2.3. Comparison with Stability Data Reported in Literature

Previous work on the stability of Ni-based catalysts is summarized in Table 2. These results can be compared with previous work on Ni-based catalysts for NH<sub>3</sub> decomposition, for example, by Okura et al.<sup>[18]</sup> who found that the catalytic activity remained unchanged over a period of 50 h.<sup>[18]</sup> If the measurement time had been 50 h for the Ni-based industrial reference catalyst presented in our work, only activation would have been observed. A similar activation of a Ni-based catalyst in NH<sub>3</sub> decomposition has also been reported by Donald et al.<sup>[19]</sup> for the decomposition of dilute NH<sub>3</sub> over a period of 10 h on the stream. Compared with previous work, the long measurement time of 800 h allowed us to detect minor deactivation of the catalyst after the initial activation that occurred during the first 250 h in the stream. Yamazaki et al.<sup>[20]</sup> investigated the long-term durability of Ru/MgO for up to 4000 h and observed a linear decrease in catalytic activity.

The high stability of the industrial reference catalyst observed in this study demonstrates the high suitability of Ni-based catalysts for long-term NH<sub>3</sub> decomposition under steady-state conditions. However, also the stability under fluctuating conditions present in future energy systems with renewable energy sources must be investigated, which will be the focus of further studies. The characterization results obtained with the less active and more strongly deactivating Ni/Al<sub>2</sub>O<sub>3</sub> catalyst prepared by co-precipitation clearly identified sintering both of the Ni

**Table 2.** Overview over stability tests using Ni-based catalysts in literature.

Material	Duration of test	Temperature	NH <sub>3</sub> mole fraction	References
	[h]	[°C]	[%]	
Layered double hydroxides derived Ni <sub>x</sub> (Mg <sub>y</sub> Al <sub>z</sub> O <sub>n</sub> )	150	550 and 620	100	[21]
90 mol% Ni on Al <sub>2</sub> O <sub>3</sub>	72	600	100	[22]
40 wt% Ni/Y <sub>2</sub> O <sub>3</sub>	50	550	100	[18]
La-modified Ni/Al <sub>2</sub> O <sub>3</sub> catalyst	15	700	100	[23]
40 wt% Ni/BaZrO <sub>3</sub>	35	550	100	[24]
CeO <sub>2</sub> modified Ni/Al <sub>2</sub> O <sub>3</sub>	180	500	15	[25]
Ni/Zr-Doped Al <sub>2</sub> O <sub>3</sub>	5	800	100	[26]
NiO/Al <sub>2</sub> O <sub>3</sub>	20	600	100	[27]
Ni/Al <sub>2</sub> O <sub>3</sub>	24	600	100	[28]

nanoparticles and of the Al<sub>2</sub>O<sub>3</sub> matrix under reaction conditions, which must be inhibited as a major task for further catalyst optimization.

### 3. Conclusion

A setup for the investigation of the long-term stability of catalysts for NH<sub>3</sub> decomposition was successfully constructed with a three-point temperature controller to ensure isothermal operation of the catalyst despite thermal effects that occur due to the changes in NH<sub>3</sub> conversion during activation or deactivation. The Ni-based reference catalyst reached a conversion of around 90% using 490 mL min<sup>-1</sup> NH<sub>3</sub> and 10 mL min<sup>-1</sup> and 500 mg catalyst at 534 °C. In comparison, a 51 wt% Ni/Al<sub>2</sub>O<sub>3</sub> catalyst prepared by co-precipitation showed lower activity with a maximum conversion of 54.1%. Initially, the conversion of NH<sub>3</sub> over the industrial catalyst was ≈80% directly after reduction, but increased to 90.1% within the first hour and further increased within the first 250 h to 91.9%. This activation process was probably caused by further reduction and restructuring of the catalyst during NH<sub>3</sub> decomposition. After 250 h TOS the conversion of NH<sub>3</sub> started to decrease slightly, and a decrease in conversion of only 1.5% relative to the maximum conversion was observed after 800 h. Over the 496 h of deactivation the catalyst seemed to deactivate essentially linearly. Overall, the Ni-based industrial reference catalyst showed high stability during long-term NH<sub>3</sub> decomposition, rendering it suitable for the application in large-scale plants. In contrast, the Ni/Al<sub>2</sub>O<sub>3</sub> catalyst deactivated over time losing 13.5% conversion over 800 h TOS. Both the Ni<sup>0</sup> nanoparticles and the Al<sub>2</sub>O<sub>3</sub> matrix were found to sinter, requiring an improvement of its high-temperature stability.

### 4. Experimental Section

**Experimental Flow Setup:** The setup consisted of a modular gas supply, a reactor unit, and the analytics. The setup was controlled via LabVIEW, and most of the valves were actuated pneumatically. Mass flow controllers from Bronkhorst were used to control the flowrates of N<sub>2</sub>, H<sub>2</sub>, Ar, and NH<sub>3</sub>. All gases were mixed via monoblock valves provided by Swagelok enabling feeding different gas compositions. Additionally, a calibration line was used to feed other gases or gas mixtures for example, for calibration purposes. NH<sub>3</sub> was taken from a gas cylinder with liquified NH<sub>3</sub> enabling the operation of the setup with a flow of 500 mL min<sup>-1</sup> NH<sub>3</sub> for 800 h with a 40 L gas cylinder or 1000 h with a 50 L gas cylinder (normal conditions: 273 K and 1 bar). The flow ranges and the purities for the used gases are summarized in Table 3.

The gas lines consisted of ¼" stainless steel tubes and were heated to 140 °C to prevent adsorption of NH<sub>3</sub> and water. The reactor was made of a ½" stainless steel tube with an inner diameter of 10.1 mm. Inside the reactor an axial tube with an outer diameter of ½" was used which served as a protective tube for four thermocouples. The reactor is shown schematically in Figure 5a.

Within the inner tube four type K thermocouples were placed to monitor the temperature along the axial coordinate (numbered 1–4). Both the inner and the outer tube were coated with Silcolloy® by SilcoTek® to prevent corrosion and blind activity of the stainless-steel walls. Within the reactor the sample was held in place by a quartz glass rod in the lower portion, a quartz glass tube in the upper portion of the reactor, and two plugs of quartz wool. The reactor with a total length of 43 cm was connected to the tubing via VCR® adapters from Swagelok®. It was possible to remove the reactor from the setup under inert conditions due to four

**Table 3.** Overview of the gas supply and gas purities.

	Gas	Purity	Flow rate
		[%]	[mL min <sup>-1</sup> ]
MFC 1	N <sub>2</sub>	99.999	0–1000
MFC 2	Calibration line	variable	0–1000 (N <sub>2</sub> )
MFC 3	Ar	99.999	0–20
MFC 4	H <sub>2</sub>	99.999	0–1000
MFC 5	NH <sub>3</sub>	99.999	0–2000
MFC 6	NH <sub>3</sub>	99.999	0–500

ball valves (two before and two after the reactor). This arrangement also ensured that the gas lines were protected when removing the reactor which is important to prevent corrosion. The reactor connections and valves were heated with heating sleeves to 140 °C. During reaction the reactor was placed in a three-zone furnace that is controlled by three PID controllers in a master–slave configuration. The temperature in the middle zone was controlled by the master PID controller, and the zones at the inlet and outlet of the reactor were controlled by two slave controllers that matched the temperature of the middle zone. It was possible to bypass by an arrangement of three pneumatic ball valves that were controlled simultaneously.

An axial temperature profile of the reactor was recorded by moving a thermocouple along the axis in 5 mm steps while 500 mL min<sup>-1</sup> N<sub>2</sub> was flowing through it. Figure 5b shows the temperature profile that was recorded for the reactor filled with SiC. The furnace was heated to 500 °C, and temperature was measured after it had reached constant values. A temperature gradient along the axis of the reactor was found with a maximum temperature difference of 10 °C. The position 0 cm is the beginning of the inner tubing and the four thermocouples positioned in the inner tubing during the reaction are positioned at 1, 3, 5, and 7 cm relative to this reference position. The temperature was lower toward the beginning of the bed and reached isothermal conditions in the upper section of the reactor. The upper 3.5 cm were isothermal with a maximum temperature deviation of 1 °C. The investigation of the temperature profile indicates that two of the thermocouples placed in the isothermal zone that ranged from 4.5 to 8 cm relative to the reference position. Accordingly, the catalyst bed with a height of 2.6 cm was positioned from 5.4 to 8 cm (Figure 5a).

**Analytics:** The setup used a multichannel analyzer (Emerson XEGP) and a gas chromatograph (Agilent 8860) for online analysis of the effluent stream. The multichannel analyzer is equipped with 4 channels, summarized in **Table 4**.

The online GC was equipped with a heated valve box. Inside the GC the sample gas was split to two columns, one to separate the permanent gases Ar, N<sub>2</sub>, and H<sub>2</sub>, and one to separate NH<sub>3</sub> and H<sub>2</sub>O. The column used to separate the permanent gases additionally had a packed column with molecular sieves acting as a guard column. The GC used He as carrier gas, Ar as an internal standard and two thermal conductivity detectors,

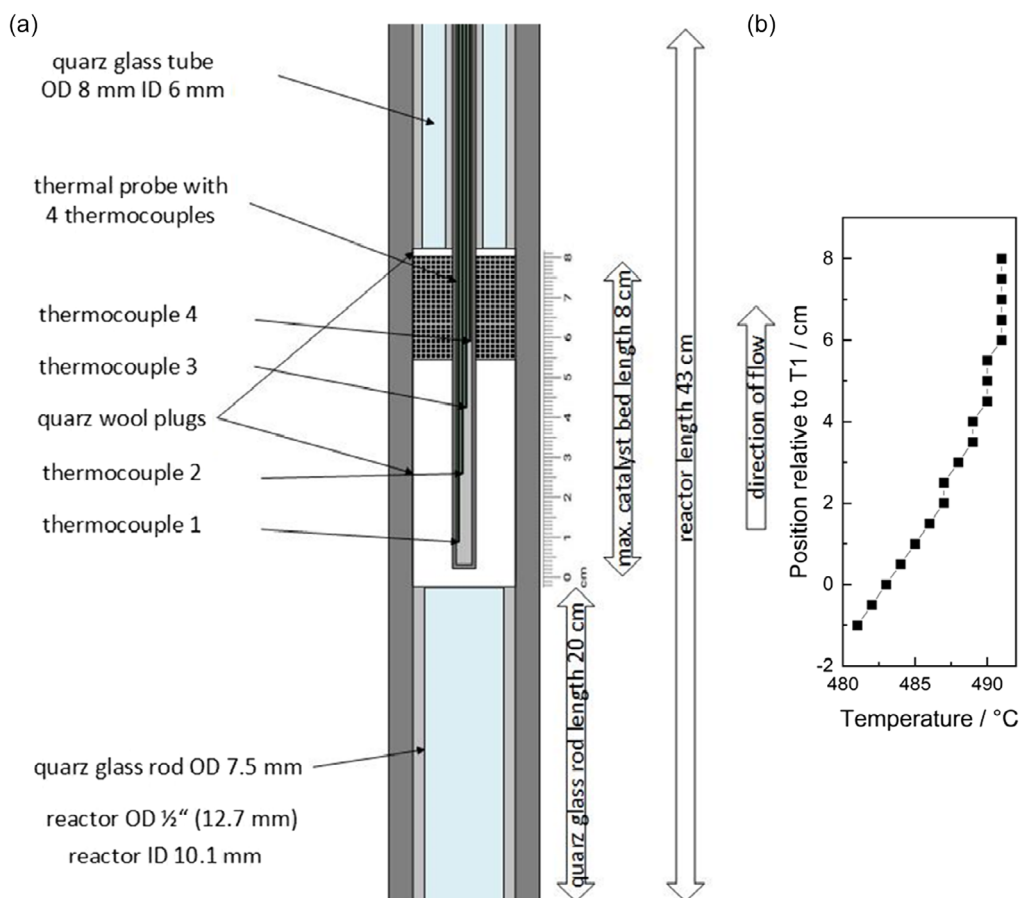


**Figure 5.** a) Reactor for long-term ammonia decomposition with four axial thermocouples and quartz parts to mechanically support the catalyst bed. b) Temperature profile of the reactor at 500 °C (setpoint). Only the upper thermocouple (4) is positioned within the middle of the catalyst bed. Profile recorded by axial movement of thermocouple inside the protective tube in 5 mm increments.

**Table 4.** Configuration of the multichannel analyzer.

Channel	Component	Measuring principle	Range
1	NH <sub>3</sub>	Infrared spectroscopy	0–100%
2	H <sub>2</sub> O	Infrared spectroscopy	0–5000 ppm
3	NH <sub>3</sub>	Infrared spectroscopy	0–3000 ppm
4	H <sub>2</sub>	Thermal conductivity	0–100%

that is one for each column. The chromatograms were analyzed using the ChemStation software (Agilent). The GC analysis was additionally used to check for undesired O<sub>2</sub> and H<sub>2</sub>O traces. The multichannel analyzer was calibrated using a two-point calibration, and the GC was calibrated for NH<sub>3</sub>, H<sub>2</sub>, Ar, and N<sub>2</sub> using a multipoint calibration with at least five points.

**Three-Point Temperature Controller:** Due to the endothermicity of the reaction the catalyst bed temperature strongly decreased under reaction conditions as a function of conversion. A three-point controller was used to adjust the setpoint for the furnace depending on the catalyst bed temperature to ensure isothermal conditions even with changing conversion. Since the three-point controller was configured in row with the PID controller of the furnace, a controlling cascade was formed for the precise adjustment of the catalyst bed temperature shown schematically in **Figure 6**.

The most upper axial thermocouple (4) was chosen for the controlling as well as the setpoint for the catalyst bed temperature and the waiting time in between cycles. The measured temperature of the bed was compared to the setpoint, and based on the deviation the furnace setpoint was adjusted in 1 °C steps. The setpoint was not changed when the desired temperature was reached within a range 0.5 °C, and visual feedback was provided in the LabVIEW program.

**Preparation of Ni/Al<sub>2</sub>O<sub>3</sub>:** All the chemicals were of analytical reagent grade. Nickel (II) nitrate hexahydrate Ni(NO<sub>3</sub>)<sub>2</sub>·6H<sub>2</sub>O (Alfa Aesar, Lot: 10 223 473), and aluminum (III) nitrate nonahydrate Al(NO<sub>3</sub>)<sub>3</sub>·9H<sub>2</sub>O (Carl Roth, Lot: 238 272 027) were used as metal salts for the preparation of the NiO–Al<sub>2</sub>O<sub>3</sub> catalyst precursor. Sodium hydroxide NaOH (Honeywell Fluka, Lot: G1340), and sodium carbonate anhydrous Na<sub>2</sub>CO<sub>3</sub> (Carl Roth, Lot: 282 317 339) were used as precipitating agents, while concentrated nitric acid solution (65 wt%, Carl Roth, Lot: 291 310 896) was used for adjusting the pH of the solution. Deionized water was obtained from a laboratory purification system (MilliQ).

A mixed metal oxide precursor with a nominal Ni content of 50 wt% was prepared by coprecipitation of a Ni–Al layered double hydroxide (internal ID: S38929) and subsequent calcination (internal ID: S39007). For the preparation of the Ni–Al layered double hydroxide (LDH), a coprecipitation was performed at constant pH in an automated laboratory reactor (Mettler-Toledo, LabMax RX-10-2 (internal ID: E19)). First, a mixed metal salt solution was prepared by dissolving 168.66 g of Ni(NO<sub>3</sub>)<sub>2</sub>·6H<sub>2</sub>O and 157.56 g Al(NO<sub>3</sub>)<sub>3</sub>·9H<sub>2</sub>O in 1000 mL deionized water, resulting in an overall metal nitrate concentration of 1M. Following this, aqueous solutions of NaOH (3 M, 1000 mL) and Na<sub>2</sub>CO<sub>3</sub> (0.5 M, 500 mL) were prepared. The LabMax reactor thermostated to 30 °C was filled with 400 mL of the Na<sub>2</sub>CO<sub>3</sub> solution and the pH of the solution was adjusted to 9.0 by manual addition of small amounts of concentrated HNO<sub>3</sub> solution under continuous stirring at 300 rpm. The automated precipitation was then started, in which the metal nitrate solution and the NaOH solution were dosed in a controlled manner via delivery pumps under continuous stirring at 300 rpm, ensuring that the pH of the precipitation solution was maintained at 9.0 (see Figure S3, Supporting Information). The greenish suspension was removed from the reactor without aging, filtered under vacuum, thoroughly washed with deionized water until conductivity was below 0.5 mS cm<sup>-1</sup>, and dried at 80 °C for 24 h. A total of 93.5 g of precipitation product was obtained. For ion exchange, 2.5 g of the dried precipitate were mixed with 15 mL deionized water and 0.25 g of Na<sub>2</sub>CO<sub>3</sub> under continuous stirring (300 rpm) at 30 °C for 2 h. The filtration, washing, and drying procedures were then repeated. The procedure was carried out seven times and the products obtained were combined, resulting a total batch of 5.3 g. Finally, 5.05 g of the ion exchanged LDH batch were calcined in a crucible placed in a quartz tube at 600 °C (heating rate: 2 K min<sup>-1</sup>) for 3 h in a flowing mixture of 21 vol% O<sub>2</sub>/Ar (total flow rate: 100 N mL min<sup>-1</sup>).

**Characterization of Ni/Al<sub>2</sub>O<sub>3</sub>:** To investigate the potential activation and deactivation of the Ni/Al<sub>2</sub>O<sub>3</sub> catalyst, TPR, XRF, N<sub>2</sub> physisorption and XRD measurements were performed with the mixed oxide precursors, freshly reduced catalyst, and spent catalyst after 1000 h of NH<sub>3</sub> decomposition and passivation using N<sub>2</sub>O/N<sub>2</sub>.

TPR experiments were conducted up to a temperature of 800 °C. 114.7 mg of the mixed metal oxide precursor was loaded into a quartz glass U-Tube reactor between two plugs of quartz wool. A thermocouple was centrally positioned within the fixed bed. The reactor was then placed in a metal block furnace and purged with 80 N mL min<sup>-1</sup> of N<sub>2</sub> (99.999%) for 2 h at 100 °C. Following purging, TPR measurements were carried out under a flow of 84 N mL min<sup>-1</sup> of 4.69% H<sub>2</sub> in Ar (both 99.999%), starting from ambient temperature and ramping up to 800 °C at a heating rate of

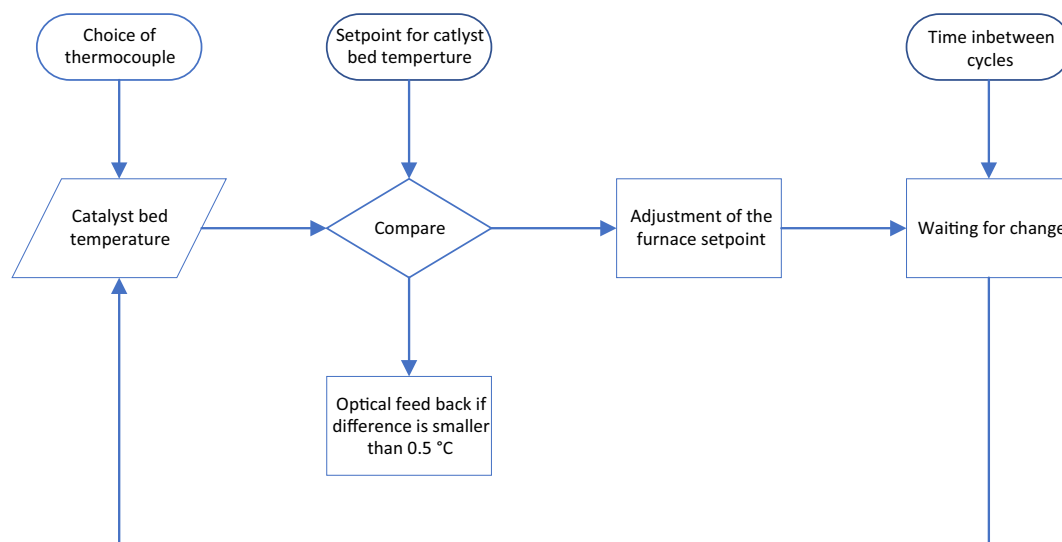


**Figure 6.** Scheme of the temperature control system used to ensure the isothermal operation of the reactor.

5 K min<sup>-1</sup>. The maximum temperature was sustained for 1 h. The effluent mole fraction of H<sub>2</sub> was determined using a thermal conductivity detector (LFE CONTHOS 3E), enabling the calculation of H<sub>2</sub> consumption during the reduction process.

N<sub>2</sub> physisorption was employed to assess the total surface area and pore size distribution of the mixed metal oxide precursor and spent catalyst after 1000 h of NH<sub>3</sub> decomposition. Prior to the N<sub>2</sub> physisorption analysis, the samples underwent pretreatment in a prep J4 instrument from 3 P Instruments at 200 °C for 2 h, reaching an end pressure of 4 × 10<sup>-3</sup> mbar. Subsequently, N<sub>2</sub> physisorption measurements were conducted using an Autosorb 6 instrument from Quantachrom. BET analysis was carried out within the range of 0.05 to 0.35 *p/p*<sub>0</sub>.

The Ni content of the calcined NiO–Al<sub>2</sub>O<sub>3</sub> mixed oxide catalyst precursor was analyzed by XRF using a commercial WD XRF S8 Tiber instrument (BRUKER AX). Approximately 0.1 g of the sample was fused with di-lithium tetraborate (8.9 g) under vacuum conditions to form a solid solution in glass.

XRD measurements of the Ni/Al<sub>2</sub>O<sub>3</sub> catalyst were conducted using a Bruker D8 DISCOVER with theta-theta geometry, Cu Kα radiation (λ = 0.15406 nm, 40 kV, 40 mA), and an energy-dispersive LYNXEYE XE-T detector. Fluorescence was automatically suppressed by the detector. The instrument was further equipped with a motorized aperture in the primary beam path and a motorized airscatter aperture above the sample holder. For the measurements conducted at ambient conditions, angles from 30° to 85° 2θ were measured with a step size of 0.020° and a time per step of 1.5 s. The samples were placed on Si single crystals and rotated during the measurements. Evaluation of the recorded diffraction patterns was performed using the DiffraC.EVA Software equipped with access to the powder diffraction file 2 (PDF-2) database provided by the International Centre for Diffraction Data (ICDD).

**Transient Experiment:** Prior to the isothermal long-term stability measurement, a transient experiment was performed to determine the conversion as a function of temperature. 500 mg of industrial catalyst sieve fraction (200–300 μm) was diluted with 4.5 g of SiC of the same sieve fraction. The mixture was filled into the reactor and reduced according to the instructions of the manufacturer. After reduction the reactor was bypassed, and the flow was adjusted to 490 mL min<sup>-1</sup> NH<sub>3</sub> and 10 mL min<sup>-1</sup> Ar (98% NH<sub>3</sub>% and 2% Ar). After a short equilibration and confirmation of the mole fractions by GC the reactor was switched online. Then, a quasi-steady-state experiment was performed using a slow heating rate of only 1 °C min<sup>-1</sup> to investigate conversion as a function of temperature and to determine the temperature necessary to reach a conversion of roughly 90%.

**Long-Term Experiment:** For the long-term experiment a new catalyst sample of both the industrial catalyst and the academic Ni/Al<sub>2</sub>O<sub>3</sub> were freshly reduced. The reduction for both catalysts was carried out accordingly to the manufacturer's instructions. After reduction the temperature was adjusted manually to match the desired catalyst bed temperature of 534 °C, and the three-point controller was switched on to ensure isothermal conditions. The temperature was chosen based on previous experiments to achieve approximately a conversion of 90% of NH<sub>3</sub>. Within the first 4.5 h the conversion of NH<sub>3</sub> was determined after 30, 120, 195, and 270 min. Then, GC measurements were performed every 4 h until 56.5 h had passed, and from that point in time every 8 h.

## Supporting Information

Supporting Information is available from the Wiley Online Library or from the author.

## Acknowledgements

Research was conducted within the AmmoRef project of the Hydrogen Flagship Project TransHyDE, which is funded by the Federal Ministry of Education and Research (Bundesministerium für Bildung und

Forschung, BMBF) with the grant number 03HY203A. We thank our partner Clariant Produkte Deutschland GmbH for providing an industrial reference catalyst.

Open Access funding enabled and organized by Projekt DEAL.

## Conflict of Interest

The authors declare no conflict of interest.

## Data Availability Statement

The data that support the findings of this study are available from the corresponding author upon reasonable request.

## Keywords

ammonia decomposition, hydrogen, industrial application, long-term stability, nickel catalysts

Received: April 2, 2024

Published online:

- [1] R. York, S. E. Bell, *ERSS* **2019**, *51*, 40.
- [2] R. M. Navarro, M. A. Peña, J. L. G. Fierro, *Chem. Rev.* **2007**, *107*, 3952.
- [3] C. M. Kalamaras, A. M. Efstathiou, *Conf. Papers Energy* **2013**, *2013*, 690627.
- [4] P. L. Spath, M. K. Mann, Life Cycle Assessment of Hydrogen Production via Natural Gas Steam Reforming, **2000**. <https://doi.org/10.2172/764485>.
- [5] I. Dincer, *Int. J. Hydrogen Energy* **2012**, *37*, 1954.
- [6] C. M. White, R. R. Steeper, A. E. Lutz, *Int. J. Hydrogen Energy* **2006**, *31*, 1292.
- [7] A. W. C. van den Berg, C. O. Areán, *Chem. Commun.* **2008**, 668. <https://doi.org/10.1039/B712576N>.
- [8] J. W. Makepeace, T. J. Wood, H. M. A. Hunter, M. O. Jones, W. I. F. David, *Chem. Sci.* **2015**, *6*, 3805.
- [9] R. Lan, J. T. S. Irvine, S. Tao, *Int. J. Hydrogen Energy* **2012**, *37*, 1482.
- [10] C. Zamfirescu, I. Dincer, *Fuel Process. Technol.* **2009**, *90*, 729.
- [11] A. Wojcik, P. Middleton, I. Damopoulos, J. van Herle, *J. Power Sources* **2003**, *118*, 342.
- [12] S. Ristig, M. Poschmann, J. Folke, O. Gómez-Cápiro, Z. Chen, N. Sanchez-Bastardo, R. Schlögl, S. Heumann, H. Ruland, *Chem. Ing. Tech.* **2022**, *94*, 1413.
- [13] F. Schüth, R. Palkovits, R. Schlögl, D. S. Su, *Energy Environ. Sci.* **2012**, *5*, 6278.
- [14] J. Humphreys, R. Lan, S. Tao, *Adv. Energy Sustainability Res.* **2021**, *2*, 2000043.
- [15] A. Boisen, S. Dahl, J. K. Nørskov, C. H. Christensen, *J. Catal.* **2005**, *230*, 309.
- [16] J. A. Rodriguez, J. C. Hanson, A. I. Frenkel, J. Y. Kim, M. Pérez, *J. Am. Chem. Soc.* **2002**, *124*, 346.
- [17] M. Thommes, K. Kaneko, A. V. Neimark, J. P. Olivier, F. Rodriguez-Reinoso, J. Rouquerol, K. S. W. Sing, *Pure Appl. Chem.* **2015**, *87*, 1051.
- [18] K. Okura, T. Okanishi, H. Muroyama, T. Matsui, K. Eguchi, *ChemCatChem* **2016**, *8*, 2988.
- [19] J. Donald, C. Xu, H. Hashimoto, E. Byambajav, Y. Ohtsuka, *Appl. Catal., A* **2010**, *375*, 124.
- [20] K. Yamazaki, M. Matsumoto, H. Kubo, T. Fujitani, M. Ishikawa, A. Sato, *Ind. Eng. Chem. Res.* **2022**, *61*, 5778.

- [21] Q. Su, L. Gu, Y. Yao, J. Zhao, W. Ji, W. Ding, C.-T. Au, *Appl. Catal., B* **2017**, *201*, 451.
- [22] Y.-Q. Gu, Z. Jin, H. Zhang, R.-J. Xu, M.-J. Zheng, Y.-M. Guo, Q.-S. Song, C.-J. Jia, *J. Mater. Chem. A* **2015**, *3*, 17172.
- [23] K. Okura, T. Okanishi, H. Muroyama, T. Matsui, K. Eguchi, *Appl. Catal., A* **2015**, *505*, 77.
- [24] K. Okura, K. Miyazaki, H. Muroyama, T. Matsui, K. Eguchi, *RSC Adv.* **2018**, *8*, 32102.
- [25] W. Zheng, J. Zhang, Q. Ge, H. Xu, W. Li, *Appl. Catal., B* **2008**, *80*, 98.
- [26] S. Henpraserttae, S. Charojrochkul, W. Klysubun, L. Lawtrakul, P. Toochinda, *Catal. Lett.* **2018**, *148*, 1775.
- [27] A.-H. Lu, J.-J. Nitz, M. Comotti, C. Weidenthaler, K. Schlichte, C. W. Lehmann, O. Terasaki, F. Schüth, *J. Am. Chem. Soc.* **2010**, *132*, 14152.
- [28] Y. Gu, Y. Ma, Z. Long, S. Zhao, Y. Wang, W. Zhang, *Int. J. Hydrogen Energy* **2021**, *46*, 4045.